Chapter

Design and Optimization of Photonics-Based Beamforming Networks for Ultra-Wide mmWave-Band Antenna Arrays

Mikhail E. Belkin, Dmitriy Fofanov, Vladislav Golovin, Yuriy Tyschuk and Alexander S. Sigov

Abstract

In this chapter, we review the worldwide progress referred to designing optical beamforming networks intended to the next-generation ultra-wideband millimeter-wave phased array antennas for incoming fifth-generation wireless systems, which in recent years is under the close attention of worldwide communication community. Following the tendency, we study in detail the design concepts below true-time-delay photonics beamforming networks based on switchable or continuously tunable control. Guided by them, we highlight our NI AWRDE CAD-based simulation experiments in the frequency range of 57–76 GHz on design of two 16-channel photonics beamforming networks using true-time-delay approach. In the first scheme of the known configuration, each channel includes laser, optical modulator, and 5-bit binary switchable chain of optical delay lines. The second scheme has an optimized configuration based on only 3-bit binary switchable chain of optical delay lines in each channel, all of which are driven by four lasers with wavelength division multiplexing and a common optical modulator. In the result, the novel structural and cost-efficient configuration of microwave-photonics beamforming network combining wavelength division multiplexing and true-time-delay techniques is proposed and investigated.

Keywords: ultra-wideband millimeter-wave antenna array, computer aided design and optimization, photonics-based beamforming network

1. Introduction

Generally, antenna unit is a requisite of any on-air radio frequency (RF) system forming its service area and bandwidth capability. At present, implementing an active phased array antenna (PAA) [1] results in remarkably increased footprint and operation flexibility thanks to electronic beam steering function, which is realized by a beamforming network (BFN). The concept of electronically beam-steered PAA was proposed for radar application more than 50 years ago [2]; and due to the limited requirements for the bandwidth, up to the first decade of this century, microwave diode- or ferrite-based phase shifters were widely used in BFN as control elements. In the course of further development of radar technology, new requirements that

arose referred to the increase in the area of PAA and the sector of beam scanning, also to the expansion of operating frequency range and instantaneous bandwidth [3]. To meet all of them in BFN based on standard phase-shifter approach, a serious barrier has arisen associated with the so-called beam squint effect, which leads to beam expansion and deflection from its intended target [1]. The search for solution of the limited instantaneous bandwidth issue led to the conclusion that the most effective way for radars, both pulsed and continuous probing, is to replace phase shifters in the PAA feed network with time-delay units, which will operate as true time delay (TTD) negating the effect of the finite fill time of PAA aperture [2].

Conceptually, the operation principles of microwave phase-shifter and TTD units are similar, since the both has to adjust a large number of antenna elements to force the electromagnetic wave to add up at a particular angle to the PAA regulating such uniquely related parameters, as phase and time delay. However, in the first case, steering is provided by changing transmission phase angle (phase of S_{21}) of a two-port network, but in the second one, by changing the length of the set of the passive microwave delay lines controlled by pin-diode or transistor switching circuits. So when implemented in the form of microstrip or coplanar microwave lines, it is possible to provide a bandwidth of up to tens of GHz. The main disadvantages of microwave TTD-based BFN are cumbersomeness and large insertion loss, the value of which can vary significantly at each step of the delay. Other shortcoming of microwave implementation of TTD BFN includes crosstalk due to leakage in the microwave switches that results in reflections and irregularities of transmission characteristics.

The progress of radar technique at the beginning of the current century has led to the emergence and development of ultra-wideband radar systems. The typical examples are radars with low probability of interception of signals in which the carrier frequency of signals is rapidly reconstructed during operation in wide ranges, or radars using ultra-wideband probing signals allowing to receive an image of the object in the microwave range and distinguish close targets [4]. In addition, a number of radio electronic systems operating in different frequency bands are installed and simultaneously function on mobile carriers, in particular, the marine ones. In such systems, the application of TTD-based BFN was the only solution, which induced the numerous researches aimed to eliminating the drawbacks noted above. One example of advanced microwave beamforming schemes became so-called Rotman lens that is compact in size and provides true time delay [2]. However, this concept suffers from various additional losses, the main mechanism among which is beam-angle-dependent scanning loss that could reduce significantly the level of the main lobe of the PAA radiation pattern. Another intriguing concept, which is widely utilizing in the modern receiving PAA, is a processing at an intermediate frequency using a digital BFN [4]. Nevertheless, in the transmission PAA, where the delay is usually introduced into the microwave path, the issue of using the digital BFN is still open.

When creating such systems, combining the demands for various components of complex radar systems and ensuring the effective implementation of the required characteristics allow the use of approaches based on microwave photonics (MWP) technologies [5, 6]. At present, for incoming communication networks of fifth generation (5G), an extremely broad instantaneous bandwidth is required too, that is why ultra-wideband phase shifting or true-time-delay techniques must be used. In addition, enlarging the operating frequency of wireless fronthaul in the millimeter range is the mainstream research topic for 5G [7], which will be addressed in detail separately. On this way, MWP approach is extremely attractive for realizing multifunction PAA's optical BFN due to its superior instantaneous operating bandwidth, immunity to electromagnetic interference, lightweight, and reconfigurability [8].

Recently, we compared by NI AWRDE-based simulation, the three versions of photonics BFN arrangements using optical phase shifters, switchable optical delay lines, and the proposed arrangement based on a combination of multichannel

fiber Bragg grating and switchable optical delay lines [9]. Continuing work of the direction, in this chapter, we review the worldwide progress referred to designing photonics-based BFN and highlight our last simulation results on design search of optimized photonics BFNs for next-generation ultra-wide millimeter-wave (mmWave) antenna arrays. In particular, Section 2 reviews the specialties of microwave and mmWave photonics technique in 5G wireless networks of radio-over-fiber (RoF) architecture. In addition, Section 3 presents theoretical background of array antenna beam steering using ideal models of phase shifters and TTD delay lines. There is a short analysis of updated photonics beamforming networks produced on optical fibers, Bragg gratings, or photonics integrated circuits (PIC) in Section 4. The principles and ways to optimize photonics BFN design is discussed in Section 5 based on the known photonics BFN scheme including set of optical delay lines and a novel structural and cost-efficient configuration that, following the results of the previous sections, consists of microwave photonics BFN using wavelength division multiplexing and TTD techniques. All schemes are modeled by NI AWRDE CAD tool. Finally, Section 6 concludes the chapter.

2. Microwave and millimeter-wave photonics technique in 5G wireless networks of RoF architecture

The next-generation wireless communications network (usually named as 5G) promises to deliver unprecedented data volumes and services for the mobile and fixed users representing both an evolution and a revolution of mobile technologies [10–13]. Some of these technologies are mainly architectural in nature—for example, moving some of the decision-making to the devices themselves (device-centric architectures and smart devices)—while others are more hardware oriented. The increasing demands for broadband services and the transmission of higher data rates have led to consideration of wireless links operating at higher carrier frequencies and extending well into the mmWave-band where total capacity of the single cell can approach some gigabits per second. **Table 1** lists three interconnected engineering challenges facing 5G [10, 14]. The first one is ultradensification of service areas and users. In the result, femtocell radio-over-fiber (RoF) architecture is proposed [15]. The second one includes utilization of mmWave spectrum [7]. Following it, microwave photonics-based circuit design comes to the forefront. At last, the third one is mobile data traffic explosion. In the result, 1000-fold factor over present-day systems must be reached.

As follows from the table, the ambitious goal to increase explosively mobile traffic is able to achieve by solving two global tasks: architectural referred to RoF and technological referred to MWP. Combining millimeter-wave band and RoF network architecture is one of the promising candidates to deliver intensive bitrate traffic with seamless convergence between optical backhaul and wireless fronthaul. In addition, RoF technique allows converting directly a lightwave spectrum to mmWave radio spectrum using a simple MWP-based up-conversion scheme [16], which is important to keep the remote cells flexible, cost effective, and power

No	Feature	Result
1	Ultra densification	Femtocell RoF architecture
2	Utilization of mmWave spectrum	Microwave photonics-based circuit design comes to the forefront
3	Mobile data traffic explosion	1000-fold factor over present-day systems

Table 1.
The key engineering challenges facing 5G.

efficient. **Figure 1** demonstrates an example of mmWave RoF architecture, which consists of central office (CO), a remote or base station (RS) and wireless subscriber terminals (ST). CO is interactively connected with RS through fiber-optic cable, and RS is interactively connected with ST through wireless link. A typical position of RS is in the center of the service area; that is, for omnidirectional covering, four PAAs with an azimuth of 90° would be an optimal decision.

As shown in a large number of studies [7, 17, 18], mmWave 5G wireless network infrastructure must be erected with a lot of small cell sites controlled by the corresponding RS. In order to avoid inter-interference in these cells, one of the promising approaches is to equip the RS with a beam-steerable PAA (as in **Figure 1**), as has been practiced in radars for many years (see section "Introduction"). According to the estimates, mmWave RS would use PAA with hundreds of antenna elements to form directional beams for transmission and to receive similar beams from adjacent STs and RSs.

To implement effective radio communication within these cells, a number of leading countries have already developed a promising spectrum including mmWave-bands up to 100 GHz. **Figure 2** exemplifies USA assignation ranged from 27.5 to 95 GHz [19]. As follows from the figure, there is a continuous operating band between 57 and 76 GHz (fractional bandwidth of 30%), which will be used by us in the following treatment.

The final topic to be highlighted in this section is to design 5G RS's equipment using microwave and mmWave photonics techniques. Microwave photonics is an interdisciplinary scientific and technological field that combines the domains of microwave engineering and photonics. This field in the last 30 years has attracted immense interest and generated many new R&Ds from both the scientific community and the commercial sector. Emerging applications for 5G networks of RoF architecture indicate that MWP is set to be a subject of increasing importance ([8, 20, 21], and refs. cited there). By common opinion, MWP technology opens the way to super-wide bandwidth transmitting characteristics at lower size, weight, and power as compared with traditional electronic approach [22]. As an example, in a typical arrangement of MWP-based microwave transmitting unit (**Figure 3**), a photonics circuit is inserted between two microwave electronic chains typically including digital-analog converter (DAC), intermediate frequency and power amplifiers (IFA and PA, respectively), and antenna. For forward and reverse transformations of microwave and optical signals, there are two interfacing units at their bounds: electrical-to-optical (E/O) and optical-to-electrical (O/E) converters. Between the interfaces, there are various photonics processing units for frequency up-conversion, filtering, time delaying, beamforming, and so on, of microwave signals in optical domain.

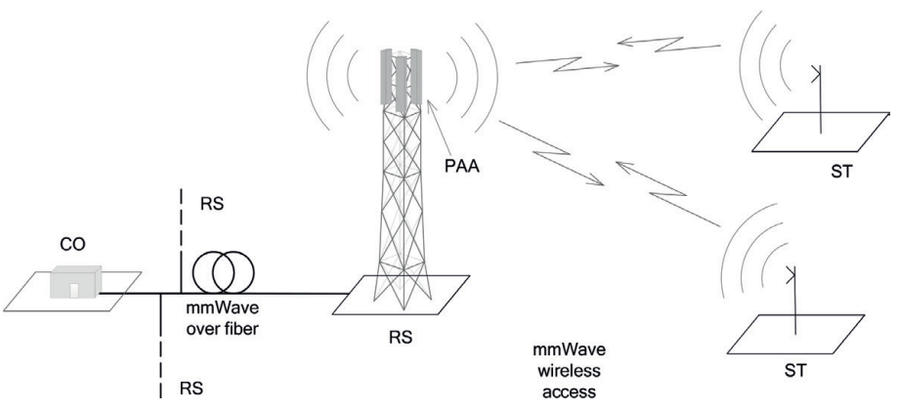

Figure 1.
An example of mmWave RoF architecture.

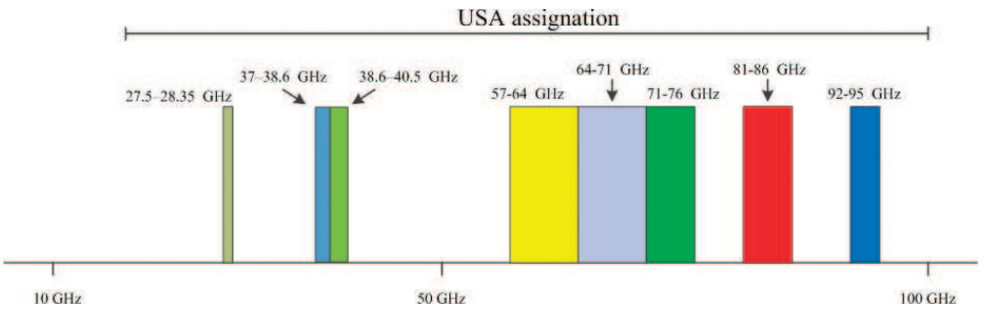

Figure 2.
5G mmWave spectrum allocation of USA assignation.

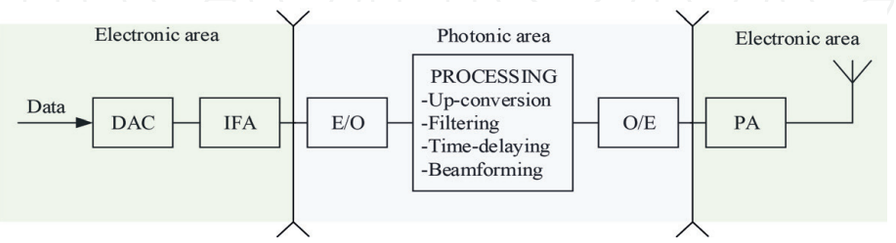

Figure 3.
A typical arrangement of MWP-based microwave transmitting unit.

The outcome. The source data for posterior calculations of PAA are:

- the operating band is 57–76 GHz (see **Figure 2**)
- the maximum azimuth steering of the main lobe deviation is ±45° (see **Figure 1**)

3. Theoretical background of array antenna beam steering

As noted in the Introduction, phased array antennas are now widely used in radar equipment due to the possibility of fast electron beam scanning and increased failure-resistant feature compared to continuous aperture antennas and mechanical scanning. The application of PAAs in radar allows achieving high speed of viewing the service area and tracking high-speed maneuvering objects [1]. Besides, PAAs ensure the operability of the radar system in a complicated interference situation due to the adaptive formation of a complex-shape radiation pattern [4]. In many cases, the use of array antenna let reduce the weight of the radar system and lower its total cost. In addition to radar, mmWave array antennas capable of operating in ultra-wide frequency range are considered as one of a key enabling technology for designing RS of 5G network, as noted in the previous section. There, a formation of a narrow steered beam by means of the antenna array makes it possible to increase the directive gain to compensate for the attenuation in the mmWave-band. Besides, the use of a narrow beam would reduce the interference effects from other closely spaced transmitters, and also provide the possibility of spatial multiplexing to increase throughput while simultaneously exchanging information with several STs.

As described above, electronic scanning in the PAA is provided by a beamforming network, which includes phase shifters, or delay lines. The BFN supports a continuous or discrete beam movement in space due to phase control or signal time delay between the array elements. Below, a short theoretical study using ideal models will be presented pursuing the goal to define the complementary input data for the posterior design of the specific photonics-based BFNs for the ultra-wide mmWave-band PAA exploiting widespread microwave-electronic computer-aided design (CAD) environment NI AWRDE.

In general, the array antenna is a collection of antenna elements connected to the transmitter/receiver through RF feeds, which includes a BFN. A typical arrangement of antenna elements is shown in **Figure 4**.

The radiation pattern of an array of identical antenna elements (Eq. (1)) is the product of the diagram of an individual element $f(\theta,\varphi)$ and the array factor $F(\theta,\varphi)$, depending on the mutual arrangement of the elements

$$D(\theta,\varphi) = f(\theta,\varphi) * F(\theta,\varphi), \tag{1}$$

where θ is an elevation angle, φ is an azimuth.
The array factor has the form:

$$F(\theta,\varphi) = \sum a_i \, exp\left(-jk\boldsymbol{r_i}\cdot\boldsymbol{r}\right), \tag{2}$$

where a_i is the transmission gain (weight) in the channel of the feed network connected to the i-th element, r_i is the radius vector of the i-th element, r is the radius-vector specifying the direction (θ,φ), k is the wave number, referred to the operation wavelength λ as $k=2\pi/\lambda$.

When analyzing various configurations of antenna arrays and feed networks, only specific variant of the array factor is often considered, assuming the antenna elements to be isotropic, with the radiation pattern $f(\theta,\varphi)=\text{const}$. In the process of the examination, the following basic parameters are analyzed: antenna directivity, mainlobe's half power or null-to-null beamwidth, beam-direction angular error, and maximum sidelobe level [1]. Radiation patterns are usually represented for the azimuth φ and elevation θ sections in a Cartesian or polar coordinate system, or in 3D form.

As mentioned above, for scanning PAAs, there are two main ways of designing the feed networks: based on phase shifters and delay lines. Mathematically, the difference between these techniques can be represented as follows. First, expanding k and multiplying radius-vectors $r_i\cdot r$, Eq. (2) can be rewritten as

$$F(\theta,\varphi) = \sum a_i \exp\left(-j\frac{\omega}{c}\boldsymbol{r_i}\cdot\boldsymbol{r}\right) = \sum a_i \exp\left(-j\omega\tau_i\right), \tag{3}$$

where ω is the angular operating frequency and τ_i is the time delay that must be introduced into the channel of the feed network connected to the i-th element to obtain the required array factor. For the narrow-band case with a central operating frequency ω_0, Eq. (3) takes the forms

$$F(\theta,\varphi) = \sum a_i \exp\left(-j\,\omega_0\tau_i\right) = \sum a_i \exp\left(-j\,\Phi_i\right), \tag{4}$$

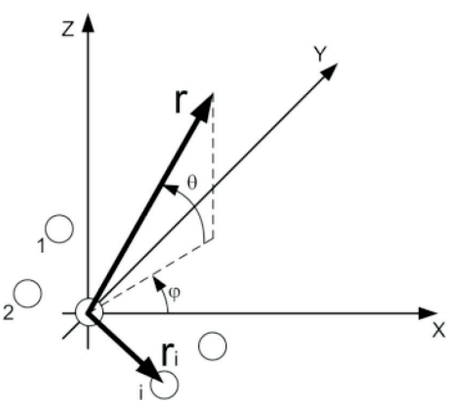

Figure 4.
Array antenna of arbitrary geometry.

where Φ_i is the phase shift, which must be introduced into the channel of the feed network connected to the i-th element, to obtain the required array factor. Obviously, if the frequency deviates from ω_0, the phase shifts in the channels of the feed network will not provide the required $F(\theta,\varphi)$. This phenomenon called "beam squint" leads to an error in the direction of the maximum of the PAA pattern, and also to a certain increase in the level of the sidelobes. Nevertheless, despite the beam squint, the BFN based on phase shifter due to the ease of implementation has become widespread in narrowband PAAs, i.e., with a fractional bandwidth, commonly not exceeding 10%, depending on the criterion used [23].

In addition, the important parameters of the PAA are the directive gain and the beamwidth closely related to it. In the simplest case of a linear equidistant array, the full width at half-maximum (FWHM) of the beam, $\Delta_{0,5}$, is inversely proportional to the aperture length L and in the antenna, broadside is determined in radians according to:

$$\Delta_{0,5} = 0.886\,\lambda/L \tag{5}$$

For an array of N elements with the distance between them of $\lambda/2$, which is often used in practice and will be considered below, Eq. (5) can be reduced to a form convenient for calculating the beamwidth in degrees:

$$\Delta_{0,5} = 101.5/N \tag{6}$$

It should be noted that the beamwidth increases with the deviation from the PAA broadside direction. For this reason, the variants of the antenna array construction are often compared along the beamwidth in the direction of the normal, taking into account the broadening effect at large deviation angles.

The directive gain, which is also considered in the direction of the broadside, and for the array of N elements, the distance, between which is equal to $\lambda/2$, is determined according to:

$$D = 2 * N, \tag{7}$$

where the factor of 2 is caused by the presence of the conducting plane in the majority of PAAs, which guides (reflects) the entire radiation flux into one half-space. In the absence of such a plane, the gain is reduced accordingly.

In the mmWave-band, it is sometimes not possible to arrange array elements at the intervals of $\lambda_{min}/2$, where λ_{min} is the minimum wavelength corresponding to the upper operating frequency. When the interval between elements in the radiation pattern increases, the grating lobes limiting the range of scanning angles might arise. Mathematically, this effect is due to the periodicity of the exponent in Eq. (2). For a linear array, the condition for the occurrence of a grating lobe in the azimuth φ with the direction of the beam φ_0 is:

$$kd(\sin\varphi - \sin\varphi_0) = m * 2\pi, \tag{8}$$

where d is the distance between antenna elements, and m is an integer. It can be shown from Eq. (2) that the range of scanning angles $\pm\varphi_{max}$ for the distance d is limited by the expression:

$$d/\lambda_{min} \leq (1 + \sin\varphi_{max})^{-1} \tag{9}$$

From Eq. (9), it follows that to ensure the absence of grating lobes when scanning in the range of $\varphi_{max} = 90^\circ$, the distance between antenna elements d should not exceed $\lambda_{min}/2$.

The phase shifters or delay lines used in BFNs can be steered continuously or in discrete steps. Because of the operation convenience, the later type is most widely exploited. Such BFNs are usually controlled by binary codes and are steered in the range from 0 to $(2^R - 1) * \delta$, where δ is the sampling period (SP) that determines the error of the BFN operation due to discreet time sampling; R is the number of bits of the binary phase shifter or delay line. For phase shifters, the parameter R is selected in such a way as to cover the phase shift range of 360° with a step δ. For delay lines, the number of bits must provide the necessary time-delay setting τ_{max} for deviating the PAA diagram by the maximum operating angle. For a given number of bits R, the SP is determined by:

$$\delta \geq \tau_{max}/(2^R - 1) \tag{10}$$

The sampling error within $\pm\delta/2$ affects primarily the direction and level of the sidelobes. For a PAA with a small number of elements, there is a primary error in the position of the beam. On the contrary, for large PAAs, the sampling error does not affect the position of the beam, since it has an average value of 0. Reducing the directivity for large PAAs due to the error of phase quantization and amplitude errors in the channels of the feed network might be described statistically in the form:

$$D = D_0/\left(1 + \sigma_\Phi^2 + \sigma_A^2\right), \tag{11}$$

where D_0 is the directivity without taking into account the quantization error, $\sigma_\Phi^2, \sigma_A^2$ are the variances of the phase quantization error or the amplitude error, respectively. Thereafter, the average level of the sidelobes might increase in more than $(\sigma_\Phi^2 + \sigma_A^2)$ times. It should be noted that the sidelobe closest to the main beam has the maximum level. Its level is determined by the distribution of the transmission gain a_i in the channels of the feed network, and for uniform distribution is –13 dB relative to the main beam level.

The influence of the PAA's parameters considered above was examined for the example of a linear equidistant array of 16 isotropic elements (**Figure 5**) designed for operation at the frequency range of 57–76 GHz. To ensure scanning without grating lobes, the distance between the elements of 2 mm was selected in accordance with Eq. (9), starting from the minimum wavelength of 4 mm. This distance leads to beamwidth of 6.3° at highest frequency and antenna gain of 15 dB in accordance with Eqs. (6) and (7), respectively.

The beam FWHM of the PAA under test varies in accordance with Eq. (5) from 8.4° at 57 GHz to 6.3° at 76 GHz. The necessity of transmitting an ultra-wideband signal with a fractional bandwidth of up to 30% by means of this PAA will inevitably lead to significant distortion of the normalized radiation pattern (NRP) shape when using a phase-shifter based BFN. We will illustrate this with the example of a signal with a 19 GHz bandwidth and a central frequency of 66.5 GHz, for which phase shifts for a beam direction of 30° are calculated according to Eq. (4). The NRPs formed by the BFN with ideal phase shifters at 57, 66.5, and 76 GHz are shown in **Figure 6**. It can be seen from the figure that the deviation of the maximum of the NRP from the desired direction is 4–6°when the frequency is varied within the operating range.

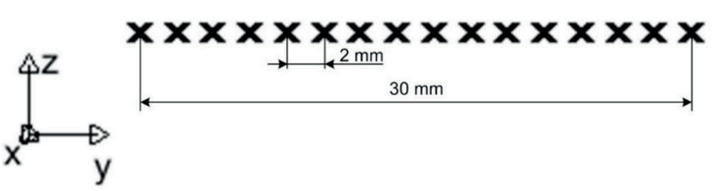

Figure 5.
Configuration of the PAA under test.

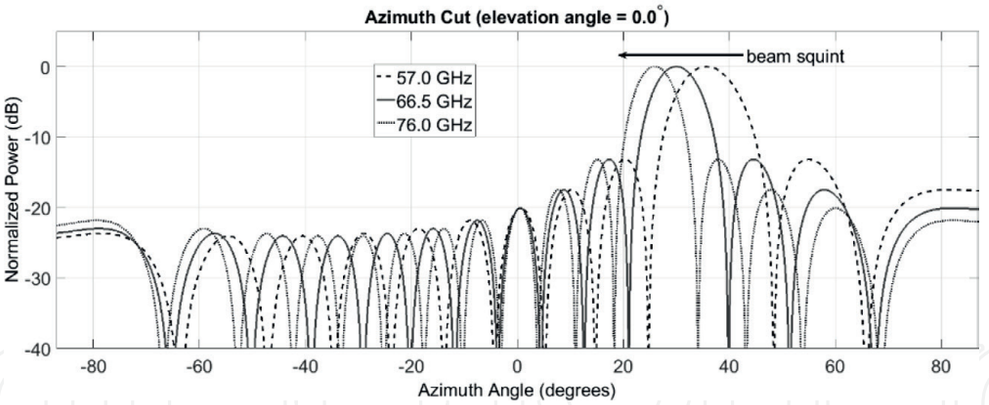

Figure 6.
Normalized radiation patterns formed by the BFN with ideal phase shifters at 57, 66.5, and 76 GHz in the case of transmitting a signal with a 30% fractional bandwidth.

Moreover, at the edges of the frequency band, the power radiated by the PAA in the given direction falls by 4 dB. Because of the squint effect, the different frequency components of the signal will be radiated in different directions. As the result, a receiver would experience a decrease in amplitude at the edges of the RF signal frequency spectrum up to 4 dB, which causes a distortion of the waveform and the occurrence of reception errors. Signal components emitted in undesired directions also might cause interference in the receivers, for which this signal was not intended. For comparison, **Figure 7** shows the NRPs formed by the BFN with delay lines at the same frequencies. It is seen from the figure that the squint phenomenon is completely absent in the entire frequency range. This well-known benefit ensures the superiority of the use of TTD-steered BFNs in PAAs with a relative bandwidth of more than 10% [23], in spite of the fact that TTD solution in principle is more expensive, bulky, and technically complex than the BFN on phase shifters. Thus, for the BFN under consideration, TTD-steered technique is the only suitable solution that ensures operability in the frequency range from 57 to 76 GHz.

Essential schematic simplification can be achieved if binary switchable delay lines (BSDL) are used instead of continuously tuned ones. To determine the parameters of such a BSDL providing scanning angle of ±45°, the maximum time delay calculated in accordance with Eq. (3) is 70.8 ps. Following Eq. (10), the use of 4, 5 and 6-bit BFNs makes it possible to obtain a sampling period of 4.7, 2.3, and 1.1 ps, respectively. The growth of SP leads to a corresponding increase of the variance for the phase quantization error, which contributes to distortions and directivity decay described by Eq. (11).

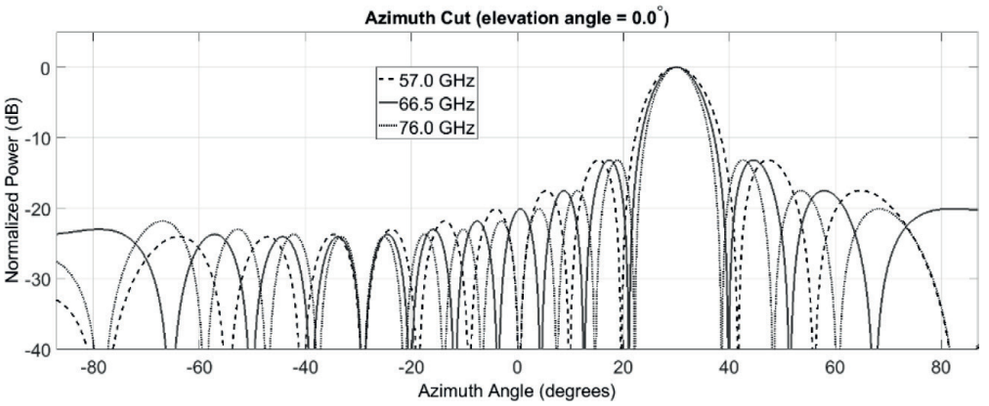

Figure 7.
Normalized radiation patterns formed by the BFN with ideal delay lines at 57, 66.5, and 76 GHz in the case of transmitting a signal with a 30% fractional bandwidth.

Number of bits	SP (ps)	Relative peak SLL (dB)	Relative average SLL (dB)
4	4.7	−3.3	−5.2
5	2.3	−8.1	−10.9
6	1.1	−10.7	−12.4

Table 2.
FoMs for BSDL with various number of bits.

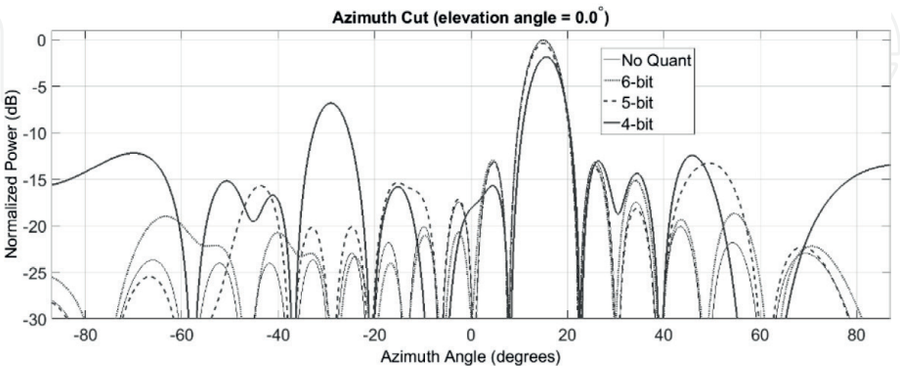

Figure 8.
Examples of radiation pattern distortion due to quantization errors.

One possible way to characterize the amount of distortion is to simulate all possible scan angles and calculate maximum sidelobe level (SLL) using the above calculated SP values [4]. Peak and average values obtained through the entire scan range can be considered as figures of merit (FoMs) that determine the performance of BSDL. **Table 2** lists the results of calculations carried out by the above technique.

Figure 8 exemplifies the distortions for BSDLs with different number of bits, which affect NRPs in different directions of scanning range.

When using a 4-bit BSDL, a sharp increase in the level of the sidelobes, a decay in directivity, and a deviation of the beam position from the desired one are observed. However, it is acceptable to use a 5-bit BSDL with a sampling period of 2.3 ps, for this case.

To summarize, the following outcomes could be concluded:

1. The use of phase shifters in ultra-wideband antenna array leads to beam squint phenomenon; so only TTD-based BFN is suitable in such case.
2. Minimum interelement distance for an array that is operable at the frequency range of 57–76 GHz without grating lobes is 2 mm.
3. The maximum time delay required to ensure scanning range of ±45° is 70.8 ps for the array under consideration and 5-bit BSDL is feasible to simplify TTD-based BFN construction. They provide a sampling period of 2.3 ps and a relative average sidelobe level of −10.9 dB over the entire scanning range (see **Table 2**).

4. Microwave photonics beamforming networks

As follows from Section 3, the optimal way to design ultra-wideband PAAs of mmWave-band is to steer the radar beam with TTD-based photonics BFN. Below, we will briefly review the current level of MWP BFN in order to select, using the data in **Table 2**, the optimal principle and scheme of its construction for efficient

No	Requirement	Result
1	Suppressing sidelobe level	Preserve the directive gain of the main beam
2	Null control	Reduce the effects of interference and jamming signals
3	Simplifying the complexity of feed network	Cost and power efficiency
4	Reducing the mutual coupling between BFN elements	Enlarge the PAA's figures of merit

Table 3.
Primary requirements to optical TTD-based microwave photonics BFNs.

No	Time-delay unit	Scheme	Bandwidth	Steering method, settling time	Delay range	Source
1	Silicon waveguide	Binary, 2 × 2 switches, MZM	8–12 GHz	Discrete <1 μs	Up to 2.5 ns	[24]
2	Linearly chirped fiber Bragg grating	TLS and separate pump laser	56 GHz	Continuously, optical pump power	200 ps	[25]
3	Dispersive fiber prism	TLS with MUX	4–8 GHz	Continuously, hopping 1 ns	—	[26]
4	Dispersive photonics crystal fibers	TLS, four fiber channels, MZM	8–12 GHz	Continuously	±31 ps	[27]
5	Match in length fibers, 5 bit	Spatial light modulators	6–18 GHz	Polarization switched, 20 ms	6–178.4 ps	[28]
6	Dispersion compensation fiber	TLS, 8 channels, MZM	8–12 GHz	Continuously	±43.3 ps	[29]
7	Holographic grating	8 × 8 2D delay matrix	18–26.5 GHz	Switchable, binary, 6-bit	443.3 ps	[30]
8	Integrated ring resonators	TLS, binary tree, 1 × 8, MZM	2.5 GHz	Continuously, thermooptical	1200 ps	[31]
9	FBG prism and fiber-optic delay lines matrix	2D, 2 × 2 switches	Narrow-band 1GHz	Switchable, sampling period 120 ps	±200 ps 360 ps	[32]
10	Integrated waveguide	Binary with 2 × 2 switches, MZM	Narrow-band, 42.7GHz	Switchable, 4 bit, 20 ns	15.7 ps	[33]
11	Integrated ring resonator-based delay lines	Binary with 2 × 2 switches, MZM	3–7 GHz	Switchable, few nanoseconds	34 ps	[33]

No	Time-delay unit	Scheme	Bandwidth	Steering method, settling time	Delay range	Source
12	TLS, integrated ring resonators	Phase modulation	3–7 GHz	Continuously	300 ps	[34]
13	Dispersion compensation fiber	TLS	5.9–17 GHz	Continuously	±200 ps	[35]
14	Linearly chirped fiber Bragg grating	Wavelength-dependent recirculating loop	11.2 GHz	Continuously	2500 ps	[36]
15	Integrated ring resonators	Binary tree, MZM	2.05 GHz	Switchable, 1 ms	630 ps	[37]

Table 4.
Examples of TTD-based photonics BFNs.

application in RSs of incoming RoF-based 5G networks. **Table 3** lists the primary requirements to a TTD-based MWP BFN from the point of view of a hardware developer for PAA.

To meet the requirements of **Table 3**, a TTD-based photonics BFN should have enough bandwidth and delay range and support small level of settling time and crosstalk. Besides, it must be either continuously tunable or switchable with a sufficiently small sampling period. At present, many implementations of TTD-based photonics BFNs exist for PAA application. Such devices are often based on a set of fiber or integrated delay lines, ring resonators, spatial light modulators, semiconductor optical amplifiers, dispersive fibers, and so on. Optical channel is usually formed based on single-carrier technique using untunable laser or on multicarrier one with wavelength division multiplexing (WDM) using tunable laser source (TLS) and spectral multiplexer (MUX). RF-to-optical conversion is advantageously realized with the help of a Mach-Zehnder intensity modulator (MZM), but other types of optical modulators are also used. For reverse optical-to-RF conversion, pin-photodiodes are exclusively utilized. **Table 4** lists the key results of our search using journal and conference contributions have been published.

As one can see from table, the developed MWP-based BFNs provide time delays from tens of picoseconds to units of nanoseconds in the bandwidth up to tens of GHz. The results being presented allow us to conclude that it is possible to meet requirements 1 and 2 of **Table 3** by using a known approach based on the concept of weighted amplitudes and phases [38]. In particular, to precisely control loss and delay time, the optical fibers of a slightly different length (example no 5) and the dispersion effect in standard single-mode (example no 3), dispersion-compensated (examples nos 6 and 13) or photonics crystal fibers (example no 4) were in use at the early stage. Later, with the development of photonics integrated technology, which ensured a significant reduction in a device footprint and simplifying the complexity of feed network (see point 3 of **Table 3**), the switchable integrated silicon waveguides (example nos. 1 and 10) or the ring microresonators (example nos 8, 11, and 15) began to be exploited. In addition, if it is necessary to ensure a continuous adjustment of the delay time, a tunable TLS (example nos 2–4, 6, 8, and 12–14) is in common use. The requirement to reduce the mutual coupling (see point 4 of **Table 3**), usually quantified as crosstalk level, occurs in common elements of

the optical channel, for example, in optical splitters or multiplexers. Its effect in photonics BFNs has been still poorly studied and will be considered in Section 5.3.

5. Principles and ways to photonics BFN design

In the process of design, a developer of new MWP-based RF apparatuses is facing a problem of choosing an appropriate software. As of today, the existing optical and optoelectronic CAD tools (OE-CAD) are not developed like being perfected for three decades CAD tools intended for modeling of RF circuits (E-CAD). On the contrary, operating at symbolic level modern high-power microwave E-CAD tool solves this problem enough simply and with high precision, but there are no models of specific active and passive photonics components in its library. To overcome this problem, we have proposed and validated experimentally a new approach to model a broad class of promising analog microwave radio-electronics systems based on microwave photonics technology. Guided by them, the electrical equivalent circuit models for the different types of semiconductor laser, photodetector, optical modulator, and so on were proposed and verified [39 and refs. cited there]. Using these components, a simple PAA's BFN was proposed and initially studied using NI AWRDE software [9]. Below, continuing work of the direction, we model a typical photonics BFN scheme including a set of switchable optical delay lines (see examples of **Table 4**), and a novel structural and cost-efficient configuration that, following the results of the previous sections, consists of microwave photonics BFN combining wavelength division multiplexing and TTD techniques.

5.1 The schematics for simulation

Figure 9 shows first photonics BFN schematic for comparison that is a part of 16-element PAA's feed network.

In this case, 16 unmodulated untunable lasers of different wavelengths λ_1–λ_{16} are used. Using the same RF signal, each transmission channel is converted by the

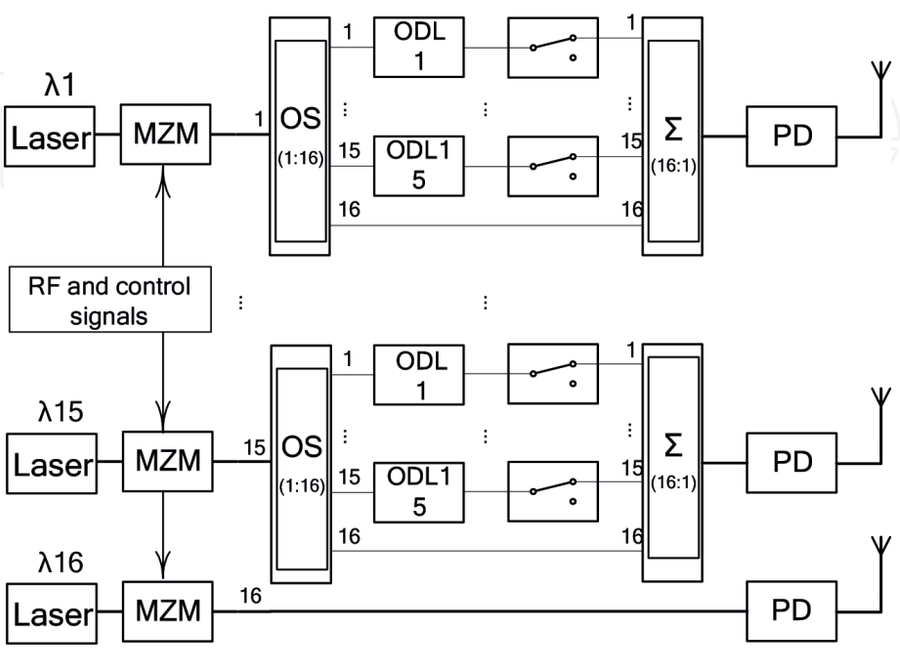

Figure 9.
16-element RF photonics BFN based on switchable optical delay lines.

corresponding Mach-Zehnder modulator (MZM) to optical range and shared into 16 branches by optical splitter (OS). Each branch consists of a switchable optical delay lines (ODL). Then, the delayed optical signals are summarized, converted into RF band by a photodiode (PD), and emitted by an ideal isotropic antenna element.

Important drawback of this scheme is the need to use a large number of lasers and MZMs (16 lasers and the same MZMs for a 16-element array), which makes it impractical due to the cumbersomeness and large energy consumption, even for such a relatively small PAA. In addition, according to the results of Section 3, each ODL must provide total delay of at least 71 ps and of digit capacity of at least 5 bits. That is, even when this BFN is implemented in the integrated version (see **Table 4**) using the waveguide material with the lowest losses [40], the difference in losses at the minimum and maximum step will be more than 30 times, which, according to Section 3, will lead to unacceptable distortions of the radiation pattern.

To overcome the above issues, **Figure 10** demonstrates an advanced photonics BFN scheme that is a part of the same 16-element PAA's feed network. In this case, only four unmodulated untunable lasers of different wavelengths λ_1–λ_4 in accordance to 200 GHz ITU WDM grid are used. Laser emissions are summarized in a spectral multiplexer (MUX), modulated in the common MZM by RF signal, and, through optical circulator, are input to four-channel reflected Bragg grating (RBG). The levels of corresponding delayed signals are recovered by an optical amplifier (OA) with an optical bandpass filter (OBF) after it, and shared into 16 branches by OS. Each branch consists of a 3-bit switchable ODL unit delayed once more optical signals for 2.3, 4.6, and 9.2 ps (see results of Section 3), a spectral demultiplexer (DMUX), 1 × 4 optical switch (OSW), a PD, and a PAA's antenna element. In addition, the schematic of 3-bit binary delay line is shown in **Figure 11**.

5.2 Models

Figures 12, **13** demonstrate the equivalent models of the BFN schemes discussed above that are developed using the NI AWRDE microwave electronic CAD tool. The proposed scheme of **Figure 13** contains two units that can be implemented based on PICs: 3-bit optical delay line and a four-channel reflected Bragg grating module. The equivalent model of the first unit is shown in **Figure 14**. The NI AWRDE equivalent model of the second one was proposed and studied in detail elsewhere [41].

5.3 Simulation experiments

With the help of the developed models, a number of simulation experiments were carried out, the main task of which was to check the stability of the proposed scheme for the nonideality of the transmission characteristics of the modules and units that make up its composition in according with the primary requirements to

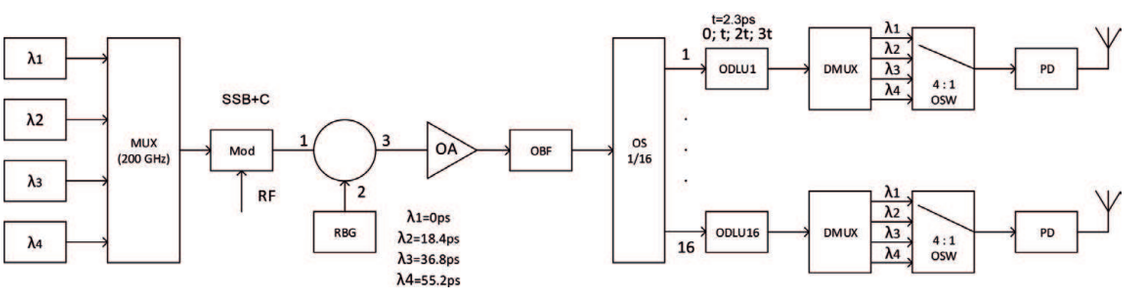

Figure 10.
16-element RF photonics BFN based on a combination of multichannel fiber Bragg grating and switchable optical delay lines.

DOI: http://dx.doi.org/10.5772/intechopen.80899

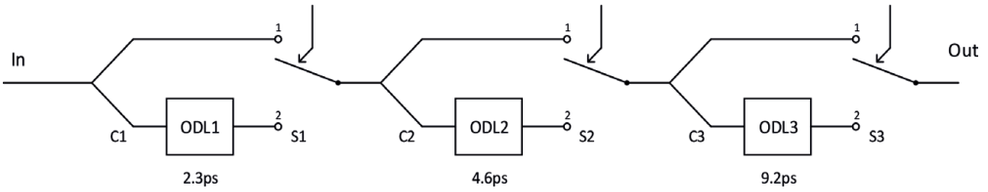

Figure 11.
The schematic of 3-bit binary delay line.

a TTD-based MWP BFN (see **Table 3**). The key parameter providing the requirements of point 4 of this table is a crosstalk interference, the permissible level of which in the TTD-based photonics BFN is still poorly studied. For example, in the scheme of **Figure 10**, there are a number of sources of crosstalk interference, including insufficient isolation of the arms of an optical circulator, an OS, and a DMUX. Experiments were carried out on the basis of specific input data received and substantiated in Sections 2 and 3. First, the known and the proposed schemes containing ideally isolated arms were modeled. A comparison of their NRPs showed

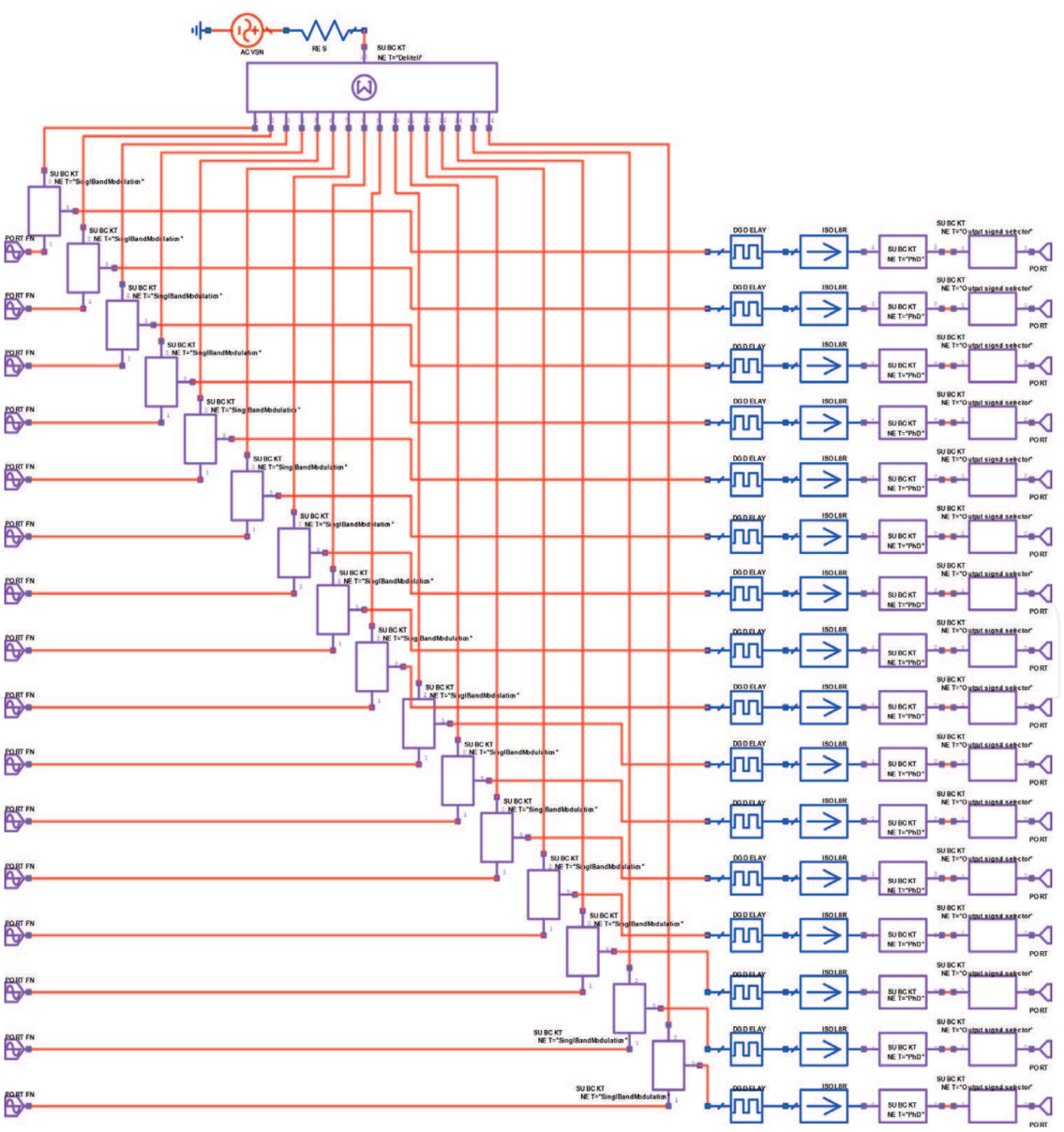

Figure 12.
NI AWRDE model of 16-element RF photonics BFN based on switchable optical delay lines.

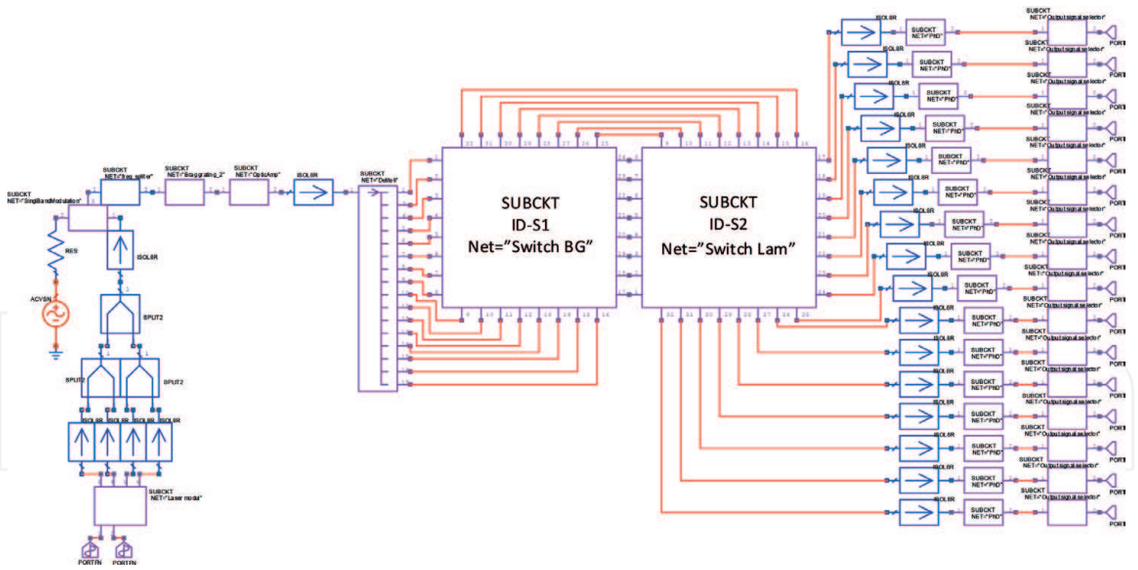

Figure 13.
NI AWRDE model of 16-element RF photonics BFN combining four-channel optical source, four-channel reflected Bragg grating, and 3-bit switchable optical delay lines.

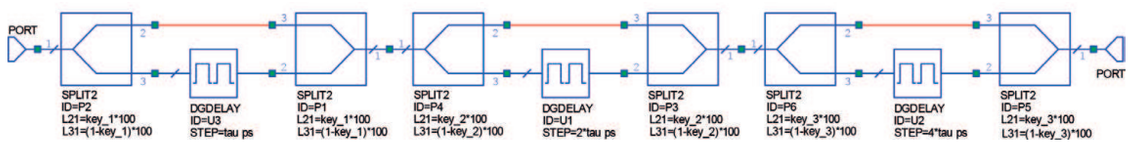

Figure 14.
NI AWRDE model of 3-bit optical delay line.

their complete identity. **Figure 15** exemplifies the calculation results of NRP characteristics for the both schemes under testing at the lower, middle, and upper frequencies of the PAA's operating range for beam deflection angles of 45° (a) and 30° (b). Comparison with the results of formal calculations given in Section 3 allows us to draw a conclusion about the correctness of the developed models.

Investigation of the effect of crosstalk interference showed the overall stability of the proposed scheme. **Figure 16** exemplifies the NRPs for the case of a joint effect of crosstalk (CS) in an optical circulator and amplitude asymmetry of the levels at the output of the optical splitter (AiOS). As on can see, their effect causes a phase shift of sidelobes, which leads to an increase in their level. However, their suppression meets the standard requirements for phased arrays.

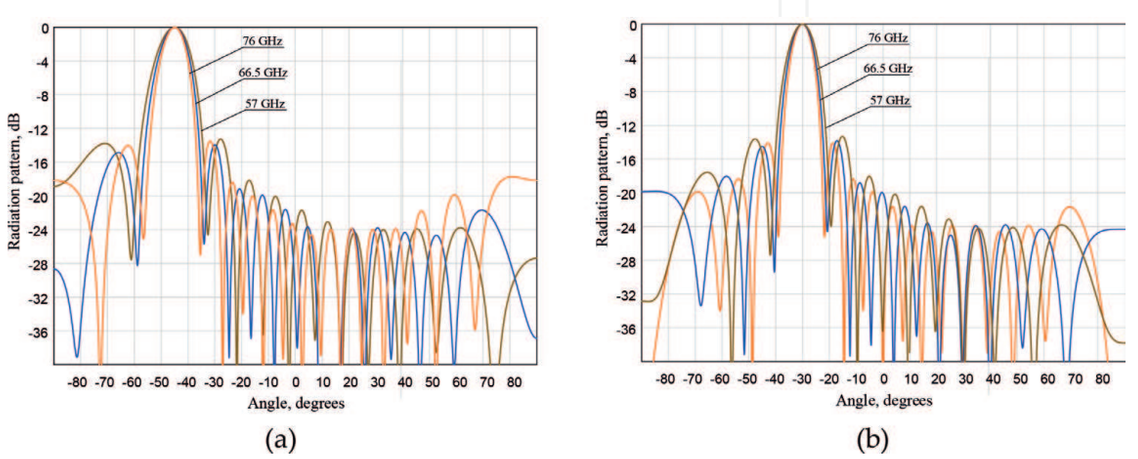

Figure 15.
Normalized radiation patterns of the both TTD-steered 16-element photonics BFNs.

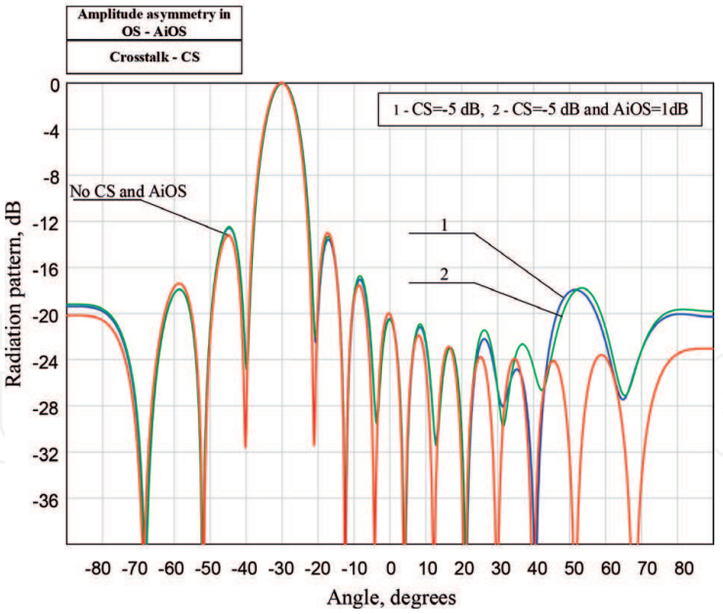

Figure 16.
Normalized radiation patterns of 16-element BFN combining 4-channel optical source, four-channel Bragg grating, and 3-bit switchable optical delay lines.

6. Conclusions

In the chapter, we explored and demonstrated the availability of using the phased array antennas, which were known for a long time in the radar technique, in the incoming fifth-generation wireless communication systems. The study was carried out using a specific example of designing a photonics-steered beamforming network (BFN) of a transmitting-phased array antenna for a remote station operating in the V-band with a 30% fractional bandwidth allocated in the USA as a promising one for future 5G systems. For this goal, we first reviewed the specialties of microwave and millimeter-wave photonics technique in 5G wireless networks of radio-over-fiber architecture. Then, to determine the input data for subsequent design, a theoretical background of array antenna beam steering using ideal models of phase shifters and true-time-delay lines was presented. A brief analysis of updated optical beamforming networks produced on optical fibers, Bragg gratings or photonics integrated circuits, showed the possibility and efficiency of constructing the delay elements required for the device being developed, on the basis of photonics integrated circuits. The developed models and executed simulation of two versions of photonics BFN based on known scheme including set of optical delay lines and a novel structurally and cost-efficient configuration using wavelength division multiplexing and TTD techniques demonstrated the advantages of the proposed scheme from the point of view of the simplicity, key figures of merit, size, weight, and power features.

Acknowledgements

This work was supported by the Russian Foundation for Basic Research, Grant No. 17-57-10002.

Conflict of interest

The authors declare the lack of the conflict of interest.

Author details

Mikhail E. Belkin[1*], Dmitriy Fofanov[1], Vladislav Golovin[2], Yuriy Tyschuk[2] and Alexander S. Sigov[1]

1 Moscow State Technological University (MIREA), Scientific and Technological Center "Integrated Microwave Photonics", Moscow, Russian Federation

2 Sevastopol State University (SevSU), Sevastopol, Russian Federation

*Address all correspondence to: belkin@mirea.ru

References

[1] Mailloux RJ. Phased Array Antenna Handbook. Boston: Artech House; 2005. 515 p

[2] Skolnik MI, editor. Radar Handbook. New York City: McGraw Hill Publishing; 2001. 1351 p

[3] Bradsell P. Phased arrays in radar. Electronics & Communications Engineering Journal. 1990;**2**(2):45-51

[4] Hansen RC. Phased Array Antennas. New Jersey: John Willey & Sons Inc; 2009. 547 p

[5] Matthews P. Practical photonic beamforming. In: Proceedings on IEEE International Topical Meeting on Microwave Photonics. 1999. pp. 271-274

[6] Seeds AJ, Williams KJ. Microwave photonics. IEEE/OSA Journal of Lightwave Technology. 2006;**24**(12):4628-4641

[7] Alavi SE, Soltanian MRK, et al. Towards 5G: A photonic based millimeter wave signal generation for applying in 5G access fronthaul. Scientific Reports. 2016;**6**:11

[8] Capmany J, Novak D. Microwave photonics combines two worlds. Nature Photonics. 2007;**1**(1):319-330

[9] Belkin ME, Golovin V, Tyschuk Y, Sigov AS. Comparison of RF photonics-based beamformers for super-wide bandwidth phased array antennas. IOP Conference Series: Materials Science and Engineering. 2017;**198**:1-4

[10] Andrews JG et al. What will 5G be? IEEE Journal on Selected Areas in Communications. 2014;**32**(6):1065-1082

[11] Chen S, Zhao J. The requirements, challenges and technologies for 5G of terrestrial mobile telecommunication. IEEE Communications Magazine. 2014;**52**(5):36-43

[12] Munn J. Our 5G future: In the fast lane with numerical simulation. Microwaves & RF. 2016;**55**(11):48-50

[13] Frenzel L. Making 5G happen. Microwaves & RF. 2017;**56**(12):1-5

[14] Boccardi F et al. Five disruptive technology directions for 5G. IEEE Communications Magazine. 2014;**52**:74-80

[15] Novak D, Waterhouse R. Emerging disruptive wireless technologies – Prospects and challenges for integration with optical networks. In: Proceedings of Optical Fiber Communication Conference. 2013. pp. 1-3

[16] Al-Dabbagh RK, Al-Raweshidy HS. 64-GHz millimeter-wave photonic generation with a feasible radio over fiber system. Optical Engineering. 2017;**56**(2):11

[17] Vook F, Ghosh A, Thomas T. MIMO and beamforming for 5G technology. In: Proceedings of IEEE International Microwave Symposium. 2014. 4 p

[18] Browne J. What role will millimeter waves play in 5G wireless systems? Microwaves & RF. 2018;**57**(4):38-42

[19] 5G Americas White Paper on 5G Spectrum Recommendations; Apr. 2017. 28 p

[20] Yao J. Microwave photonics. Journal of Lightwave Technology. 2009;**27**(3):314-335

[21] Urick VJ, McKinney JD, Williams KJ. Fundamentals of Microwave Photonics. New Jersey: Hoboken; 2015. 489 p

[22] Paolella AC, De Salvo R, Middleton C, Logan C. Direction in radio frequency photonic systems. In: WAMICON 2015: Proceedings of the IEEE 16th Wireless and Microwave Technology Conference. Cocoa Beach, Fl, USA. 6 p

[23] Frank J. Bandwidth criteria for phased-array antennas. In: Oliner A, Knittel G, editors. Phased-Array Antennas. Dedham, MA: Artech House; 1972. pp. 243-253

[24] Fathpour S, Riza NA. Silicon-photonics-based wideband radar beamforming: Basic design. Optical Engineering. 2010;**49**(1):018201. 7 p

[25] Shahoei H, Li M, Yao JP. Continuously tunable time delay using an optically pumped linearly chirped fiber Bragg grating. Journal of Lightwave Technology. 2011;**29**(10):1465-1472

[26] Vidal B, Mengual T, Marti J. Fast optical beamforming architectures for satellite-based applications. Advances in Optical Technologies. 2012;**2012**:5. Hindawi Publishing Corporation

[27] Jiang Y, Howley B, Shi Z, et al. Dispersion-enhanced photonic crystal fiber array for a true time-delay structured X-band phased array antenna. IEEE Photonics Technology Letters. 2005;**17**(1):187-189

[28] Vodjdani N, Granger G, Mongardien D, Enard A, Fourdin C, Chazelas J. 8 channels, 5 bits wideband optical beam steering up to Ku band. In: International Topical Meeting on Microwave Photonics. 2003. pp. 389-391

[29] Shi N, Li M, Deng Y, Zhang L, Sun S, Tang J, et al. Experimental demonstration of a multi-target detection technique using an X-band optically steered phased array radar. Optics Express. 2016;**24**(13):14438-14450

[30] Yihong C, Chen RT. A fully packaged true time delay module for a K-band phased array antenna system demonstration. IEEE Photonics Technology Letters. 2002;**14**(8):1175-1177

[31] Zhuang L et al. Ring resonator-based single-chip 1 × 8 optical beam forming network in LPCVD waveguide technology. In: LEOS Benelux Proceedings. 2006. pp. 45-48

[32] Jung BM, Yao J. A two-dimensional optical true time-delay Beamformer consisting of a fiber Bragg grating prism and switch-based fiber-optic delay lines. IEEE Photonics Technology Letters. 2009;**21**(10):627-629

[33] Piqueras MA et al. Optically beamformed beamswitched adaptive antennas for fixed and mobile broadband wireless access networks. IEEE Transactions on Microwave Theory and Techniques. 2006;**54**(2):887-899

[34] Zhuang L et al. On-chip microwave photonic beamformer circuits operating with phase modulation and direct detection. Optics Express. 2014;**22**(14):17079-17091

[35] Yang DH, Lin WP. Phased-array beam steering using optical true time delay technique. Optics Communication. 2015;**350**:90-96

[36] Zhang J, Yao J. Photonic true-time delay Beamforming using a switch-controlled wavelength-dependent recirculating loop. Journal of Lightwave Technology. 2016;**34**(16):3923-3929

[37] Zhuang L et al. Novel ring resonator-based integrated photonic beamformer for broadband phased array receive antennas— Part II: Experimental prototype. Journal of Lightwave Technology. 2010;**28**(1):19-31

[38] Mohammed JR, Sayidmarie KH. Synthesizing asymmetric SideLobe pattern with steered nulling in non-uniformly excited linear arrays by controlling edge elements. International Journal of Antennas and Propagation. 2017;**2017**. Article ID 9293031, 8 pages

[39] Belkin ME, Golovin V, Tyschuk Y, Vasil'ev M, Sigov AS. Computer-aided design of microwave-photonics-based RF circuits and systems. In: Loo XS, editor. RF Systems, Circuits and Components. United Kingdom: IntechOpen Publishing. 20 p. (in print)

[40] Zhuang L et al. Low-loss, high-index-contrast Si3N4/SiO2 optical waveguides for optical delay lines in microwave photonics signal processing. Optics Express. 2011;**19**(23):23162-23170

[41] Belkin ME, Golovin V, Tyschuk Y, Sigov AS. A simulation technique for designing next-generation information and communication systems based on off-the-shelf microwave electronics computer tool. International Journal of Simulation and Process Modelling. 2018;**13**(3):238-254